Assimilation of mid-depth velocities from Argo floats in the western South China Sea

Pinqiang Wang[1], Weimin Zhang[1,2], Huizan Wang[1], Haijin Dai[1], Xiaohui Wang[1,3]

1. College of Meteorology and Oceanography, National University of Defense Technology, Changsha, China, 410073
2. Laboratory of Software Engineering for Complex Systems, Changsha, China, 410073
3. Delft Institute of Applied Mathematics, Delft University of Technology, Delft, Netherlands

Corresponding author address: W. Zhang, College of Meteorology and Oceanography, National University of Defense Technology, Deya Road, Changsha, China, 410073. Email: wmzhang104@139.com

Abstract

Argo floats provide massive temperature (T) and salinity (S) profiling observations of the upper ocean, which are widely used in ocean data assimilation. However, previous studies are mainly limited to T/S profiling data assimilation, while data assimilation based on Argo float trajectory information has received less research focus. In this study, a new method was proposed to assimilate Argo trajectory data: mid-depth velocities are estimated from Argo trajectories and subsequently assimilated into the Regional Ocean Model System (ROMS) Model using 4DVAR (4-dimensional variational) method. This method can avoid a complicated float trajectory model in direct position assimilation. The two months assimilation experiments in South China Sea (SCS) showed that this proposed method can effectively assimilate Argo trajectory-derived mid-depth velocity data into the model and adjust the unbalanced component in the velocity increments better than the traditional ocean data assimilation, which only assimilates satellite observations and T/S profiling data. The assimilation of the Argo trajectory-derived mid-depth velocity with traditional ocean data assimilation (assimilation of satellite observations and T/S profiling data) together yielded the best performance, and more consistent with the Argo float trajectories. In addition, this method will not decrease the assimilation performance of other observations (i.e., SLA, sea surface temperature (SST), and T/S profile), which is indicative of compatibility with other observations in the 4DVAR assimilation system.

Keywords: Argo trajectory, data assimilation, mid-depth velocity, western South China Sea

1 Introduction

As the largest marginal sea in the west Pacific Ocean, the South China Sea (SCS) is strongly influenced by the wind, which has intraseasonal variations. As a result, the upper layer circulation of the SCS is characterized by anticyclonic circulation in the southern SCS, cyclonic circulation in the northern SCS during summer and cyclonic circulation during winter because of the wind direction reversal (Wyrtki 1961; Hu et al. 2000; Liu et al. 2008). The intermediate and deep current structures are poorly understood and less studied than the upper circulation due to the lack of observations. The intermediate (500m-1500m) circulation studies are mainly based on the diagnosis of hydrography data (Chu 2000), numerical simulations (Chao et al. 1996; Yuan 2002) and some *in situ* observations (Liao 1996). The circulation in the middle layer (500m-1500m) of the SCS appears as an overall anticyclonic circulation, driven by the outflow from the SCS to the Pacific Ocean in the Luzon Strait (Yuan 2002). However, the intermediate circulation still lacks accurate description due to the lack of comprehensive *in situ* observations and the numerical model drawbacks.

Strong western boundary currents (Fang et al. 2012; Wang et al. 2013; Quan et al. 2016) and mesoscale eddies (Wang et al. 2003; Xiu et al. 2010; Chen et al. 2011; Li et al. 2011; Lin et al. 2015; Zhang et al. 2016) could also be easily detected from the surface observations, i.e., many mesoscale eddy activities are observed east of Vietnam. However, some mesoscale eddies appear in the subsurface and could not be observed on the surface (Song et al. 2018). Two anticyclonic eddies were detected in the

subsurface of the southern SCS with *in situ* hydrography data (Zhang et al. 2014). Chen et al. (2015) found a mesoscale eddy in the deep layer of the northwestern SCS with mooring ADCPs. How the current numerical model captures the structure of the mesoscale eddy in the subsurface needs to be studied.

An effective tool to improve our understanding of oceanography (i.e., intermediate circulation or mesoscale eddy) is data assimilation, which combines limited observations and numerical model. The previous ocean data assimilation in the SCS is mostly based on satellite data and *in situ* T/S profiling data and mainly improves simulation of the temperature and salinity fields in the upper 1000 m. Data assimilation for the velocity field in the middle layer is usually neglected in the SCS due to a lack of velocity observations.

The international Argo program, which has been implemented since 2000, has enriched the number of observations in the middle layer to a certain extent (Wang et al., 2012a, b). Currently, the number of active floats in the global ocean is approximately 3900. Despite monitoring of the temperature and salinity in the upper ocean, the Argo float trajectory data also provide another way to study the current structure in the middle layer of the ocean (Park et al. 2004).

In the Mediterranean Forecasting System (MFS), the position information of the Argo trajectories has been directly assimilated with other observations (i.e., sea surface height (SSH), SST, and T/S profiles). Retaining the state of the upper layer, simulation of the velocity structure at parking depth could be improved by 15% with Argo float

trajectory data assimilation (Taillandier et al. 2006a, b; Nilsson et al. 2011, 2012). Instead of assimilating the original trajectory directly, we estimate the mid-depth (~1200m) velocity field from the Argo float trajectory and then assimilate the estimated velocity observation into the model. Since the velocity is already included in the ocean model, the usage of mid-depth velocity observations allows us to forgo additional trajectory prediction models, which is a difficult task. In addition, the assimilation of Argo trajectories has not yet been used in the SCS, which is another focus of this study.

The study is organized as follows: In Section 2, the mid-depth velocity estimation method from Argo trajectories and corresponding quality control are introduced. In Section 3, the experimental setup of ocean data assimilation for the estimated velocity at the parking depth is described. In Section 4, the simulation results are analyzed. Finally, a conclusion and suggested corresponding future work are presented in Section 5.

2 Velocity retrieval and 4DVAR

The Argo trajectory assimilation method is composed of the estimation and assimilation of mid-depth velocity. In this method, the quality control and observation error estimation of the velocity data are two important aspects. The assimilation technique uses 4-dimensional variational data assimilation (4DVAR). The background error covariance in 4DVAR is implicitly developed with the ocean state during the assimilation time window; thus, 4DVAR is more suitable than 3DVAR for data assimilation of sparse velocity observations.

2.1 Mid-depth velocity retrieval

Several methods have been provided to estimate the velocity at parking depth (Park et al. 2005; Xie and Zhu 2008; Lebedev et al. 2007; Ollitrault et al. 2013), which was then applied to estimate the regional or global ocean circulation at the basin scale (Voet et al. 2010; Park and Kim 2013; Ollitrault and ColindeVerdiere 2014; Markova and Bagaev 2016; Wang et al. 2018). In this paper, the method provided by Park et al. (2005) is adopted due to the method's high level of accuracy.

A complete cycle (i.e., *n*th cycle) for one Argo float is described as follows: the Argo float begins to dive at a location of P_{DS}^{n} (descent start position) by the time of T_{DS}^{n} (descent start time), then, Argo drifts within the subsurface for a long period and back to the surface at the location of P_{AE}^{n} (ascent end position) by the time of T_{AE}^{n} (ascent end time); finally, Argo drifts at the surface for a short time and transmits data. The total distance the Argo movement under water during this cycle is written as follows:

$$D_{DS\_AE}^{n} = V_{deep}^{n} \cdot \Delta T_{DE\_AS}^{n} + \int_{\Delta T_{des}} V_{des}^{*n}(z)dt_{des} + \int_{\Delta T_{asc}} V_{asc}^{*n}(z)dt_{asc} \quad (1)$$

where $D_{DS\_AE}^{n} = P_{AE}^{n} - P_{DS}^{n}$ is the total distance within the subsurface. $V_{des}^{*n}(z)$ and $V_{asc}^{*n}(z)$ are the velocity shear during descending and ascending processes, respectively. $\Delta T_{DE\_AS}^{n}$, ΔT_{des} and ΔT_{asc} are the time period during subsurface drifting and descending and ascending processes, respectively. The total time in the subsurface is $\Delta T_{DE\_AE}^{n} = \Delta T_{DE\_AS}^{n} + \Delta T_{des} + \Delta T_{asc}$. The subsurface velocity (V_{deep}^{n}) at the parking depth is written as follows:

$$V_{deep}^{n} = \frac{P_{AE}^{*n} - P_{DS}^{*n}}{\Delta T_{DE\_AE}^{m}} + E_{AE}^{n} - E_{DS}^{n} - E_{T}^{n} \quad (2)$$

P_{DS}^{*n} and P_{AE}^{*n} are estimations of P_{DS}^{n} and P_{AE}^{n}, according to the method used in Park et al. (2004). E_{AE}^{n} and E_{DS}^{n} are the errors due to the inaccuracy of P_{DS}^{n} and P_{AE}^{n}, respectively. E_{T}^{n} is the error related to velocity shear. Previous studies suggested that the total error ($E_{AE}^{n} - E_{DS}^{n} - E_{T}^{n}$) is small (~0.2 cm/s, Park et al. 2005), which confirms the accuracy of the estimated velocity.

2.2 Quality control procedure for velocity

Before assimilation into the model, two rounds of quality control are employed for higher velocity accuracy. The first round of quality control is applied to the original trajectories of the Argo float before velocity estimation, which is completed in four steps (Wang et al. 2018). The first step is removing the points if the distance between two adjacent points is larger than 1.5°; the second step is eliminating data if the time does not satisfied $T_{N}^{n-1}<T_{DS}^{n}<T_{AE}^{n}<T_{1}^{n}$ ($T_{N}^{n-1}$is the last satellite positioning point in the *n*-1th cycle and T_{1}^{n} is the first satellite positioning point in the *n*th cycle); in the third step, data are discarded if the satellite observational position is less than one in the *n*th cycle; and in the fourth step, the time information of the nearest satellite position is used if T_{DS}^{n} or T_{AE}^{n} is missing.

The second round of quality control is applied to the velocity at parking depth, which is finished in two steps. The first step is discarding data with a speed of less than 1 cm/s, which is comparable to the total error defined in Section 2.1 (approximately 0.2 cm/s) (Park et al. 2005). The second step is discarding velocity if the parking depth

changed dramatically during the adjacent cycle (for example, the parking depth jumped from 1200m to several hundred meters suddenly, and jumped back to 1200m).

After quality control, the mid-depth velocities have been used to estimate the intermediate current structure of the basin scale in the SCS (Wang et al. 2018). The climatological circulation pattern at 1200m is cyclonic in NSCS. The RMSE of mid-depth velocities with YoMaHa'07 product is 1.28 cm/s for zonal and 1.11 cm/s for meridional (Wang et al. 2018).

2.3 SCS 4DVAR system and observation errors

The SCS 4DVAR assimilation system was based on the primal formulation of incremental strong constraint 4D-Var in the Regional Ocean Modeling System (ROMS-IS4DVAR) (Moore el al. 2011a, b). The ROMS-IS4DVAR system can assimilate different types of observations (i.e., CTD, XTB, drifter, Argo, and satellite). A more detailed description of the theory, methodology and balance operator could be found in Counter et al. (1994) and Weaver et al. (2003,2005).

The mid-layer velocity obtained in section 2.1 is time averaged velocity during the drifting period in the subsurface instead of the instantaneous velocity. Correspondingly, the background field should also use the time averaged velocity field during the same parking period, which is difficult to satisfy due to the variation in the drifting period for different Argo floats. As an alternative choice, the middle time and position during the drifting period is considered to be the observation time and position in this study.

The observation errors are assumed to be uncorrelated at any time or at any point as defined in most ocean data assimilation systems. The variances along the main diagonal of observation error covariance are a combination of measurement error and representative error. Measurement errors from different data sources are obtained with the following standard deviations (Moore et al. 2011b): 2 cm for SSH; 0.4 °C for SST; 0.1 °C for *in situ* temperature (T); and 0.01 PSU for *in situ* salinity (S).

For the mid-depth velocity, the observation error are estimated through HYCOM-NCODA (HYbrid Coordinate Ocean Model - Navy Coupled Ocean Data Assimilation) product (as shown in Fig. 1). Most of the misfits are distributed between ±5 cm/s (accounting for approximately 83% of the total number), and the standard deviation of these misfits (between ±5 cm/s) is on the order of 2 cm/s. Thus, the observation error has been tested with standard deviation 2 cm/s and 5 cm/s for the 2-month assimilation. The total root mean square errors (RMSEs) and correlation coefficients (CCs) of the mid-depth (*u*, *v*) with Argo trajectory-derived velocity data are shown in Fig. 2 (since there are no direct velocity observations, the mid-depth velocities from the Argo trajectories are used as the true velocities). As the 2 cm/s velocity error showed a better performance than the 5 cm/s velocity error, with smaller RMSEs (2.6 cm/s for u and 2.8 cm/s for v) and higher CCs (0.66 for u and 0.69 for v). The standard deviation of the mid-depth velocity observation error is set to 2 cm/s in this study.

3 Experimental setup for trajectory-derived velocity assimilation

The western SCS is characterized by a dominant western boundary current

(SCSWBC) and an active mesoscale process. The mean speed is approximately 12~16 cm/s at 1000 m in the western SCS (Zhou et al. 2010). When an Argo float moved to the western SCS, the Argo float was easier to be captured by the dominant processes. Thus, the western SCS is selected as the area in which to study the impact of the Argo trajectory data assimilation on the mid-depth current structure. During the study period, No. 5903457 had just moved into the western SCS and therefore it was studied with an intense focus.

3.1 Model configuration

The Generic Length Scale (GLS; Warner et al. 2005), k–ω vertical mixing scheme, harmonic horizontal viscosity (mixing coefficient: 4 m^2 s^{-1}), no slip boundary conditions, quadratic bottom friction (bottom drag coefficient: 2.5×10^{-3}) and sponge layer are employed as the SCS ROMS model configuration. The model domain covers part of the northwestern Pacific Ocean (99°E~134°E, 1°N~30°N) with a horizontal resolution of 1/10° and 24 vertical levels. The bathymetry is derived from GEBCO08 with a minimum depth of 10 m and a maximum depth of 5500 m (Fig. 3).

The model is initialized from climatological Simple Ocean Data Assimilation (SODA) data and is forced by a climatological forcing (COADS) for 10 years, which is considered to be the model spin-up process. Then, the model is integrated for the period of 2000-2015, which is forced by real surface forcing and boundary conditions. The heat and freshwater fluxes are extracted from ECMWF's ERA-interim dataset with a horizontal resolution of 0.75° and a temporal resolution of 6 hours (Dee et al. 2011).

The wind stresses are calculated using the bulk formula with 10-meter U-wind and V-wind components from the CCMP 2.0 version (Atlas et al. 2011) with a horizontal resolution of 0.25° and a temporal resolution of 6 hours. The southern, eastern and northern boundaries adopt open boundary conditions from SODA version 3.3.1 (Carton et al. 2018), while the west boundary is closed. In detail, Radiation and Nudging boundary conditions are chosen as the 3D variables (i.e., u, v, temperature and salinity), Flather boundary conditions are chosen for the depth-integrated velocity components, and Clamped boundary conditions are chosen for the free surface.

The velocities from the Argo trajectories include the tidal current information. However, it is challenging for assimilating altimetry data into a model include tide, since tides are high frequency signal compared to the mesoscale variability. Xie et al (2011) compared the model fields with or without tides, the differences is minor on monthly averaged velocity field and the influence on temperature and salinity decreased with depths below 100m. For simplicity, tides exclude in the model in this study.

3.2 Data

The observations used in the data assimilation experiments are satellite altimeter data (SSH), satellite sea surface temperature (SST), *in situ* T/S profiling data and Argo trajectory-derived mid-depth velocity data. The SSH data are delayed time, and gridded maps of sea level anomaly (MSLA) data from AVISO (before 2016, http://www.aviso.oceanobs.com/duacs/). The blended SST data used in the experiments

are Version 2 AVHRR-only products produced by NOAA (Reynolds et al. 2007; ftp：//eclipse.ncdc.noaa.gov). Both SSH and SST data are available every day with a horizontal spatial resolution of 0.25°. The *in situ* data are the quality-controlled temperature and salinity profiles from the ENSEMBLES project (EN4) provided by the UK Met Office Hadley Center (Good et al. 2013; http://hadobs.metoffice.com/en4/download.html, Fig.5a). Before assimilated into the model, the T/S profiles were interpolated to 23 z-levels: -5 m, -10 m, -15 m, -20 m, -25 m, -30 m, -35 m, -40 m, -50 m, -60 m, -75 m, -100 m, -125 m, -150 m, -200 m, -250 m, -300 m, -400 m, -500 m, -600 m, -800 m, -1000 m, and -1200 m. This interpolated data may cause redundancy somewhere due to the ROMS terrain-following coordinate system. However, some error data in a single profile will be eliminated simultaneously. The Argo trajectory data were provided by the Coriolis Operational Oceanography data center (ftp://ftp.ifremer.fr/ifremer/argo).

3.3 Experimental design

Four experiments were designed to evaluate the Lagrangian velocity assimilation influence on the model forecast (Table 1). The reference experiment does not assimilate any data (Ctrl). In Exp1, only satellite data (SST and SLA) are assimilated. In Exp2 both satellite data and *in situ* T/S profile data are assimilated. In Exp3, additional Argo trajectory-derived mid-depth velocities are added to the Exp2 dataset. In Exp1 to Exp3, the assimilation window is 4 day. All experiments begin from the same initial

conditions (model's the real forecast on 1 January, 2013) and are driven by the same surface forcing and boundary conditions. To investigate the effects of assimilating different data, the climatological nudging should be closed in all assimilation experiments.

In all assimilation experiments, observations are continuously assimilated into the model. The assimilation procedure is shown in Fig.4, in one cycle, (for example, 2013010 to 20130105,) the model integrate from 20130101 to 2013015 (denoted as Prior) to provide background fields and extract model value in observation space. After assimilation, the model initialized from the analysis field at 20130101 and integrated to 20130105 again (denoted as Posterior). In next cycle (20130105-20130109), the model starts from the end states (20130105) of last cycle (20130101-20130105). This progress will be repeated until the end. Due to the high cost of 4DVAR calculations, all experiments were conducted for two months, with totally 15 data assimilation cycles during two months.

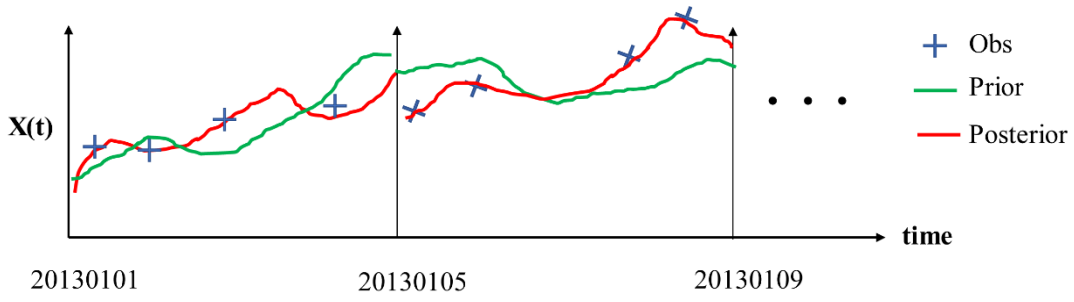

Fig.4 The process of data assimilation

4 Results analysis

After quality control, the total amount of mid-depth velocity observations in

January and February 2013 is 382 (Fig. 5a). The mean depth of Argo parking levels is 1179 m, and the amount of parking depths that are greater than 1100 m is 358 (accounting for ~94% of the total number). The mean speed is 3.4 cm/s with a maximum speed of 13.1 cm/s. Although there are a few mid-depth velocities, the impact of assimilating mid-depth velocities can transmit in time and space in 4DVAR system. The Argo floats were mainly distributed in the northern SCS. The velocity field estimated from the Argo trajectories is irregular in the middle layer (Fig. 5a). However, Fig. 5b shows that the No. 5903457 float completed a cycle near the east coast of Vietnam in Jan-Feb 2013. The following analysis is mainly based on the No. 5903457 float (Fig. 5b).

4.1 The impacts of different assimilation experiments in the western SCS

The impacts of assimilating different observations were compared based on the 2-month averaged current structure at 1200 m depth, as shown in Fig. 6. An anticyclonic eddy appeared at ~14°N in all experiments, while apparent differences are identified, such as eddy radius, position of eddy center (EC) and speed. In all experiments, the atmosphere forcing and open boundary conditions are the same, and the only difference is the observations for assimilation. The observation influences on mid-depth velocity field are introduced into the model through the balance operator. The velocity fields can be corrected by assimilating the SSH and T/S observations, which were adjusted through barotropic and baroclinic geostrophic balance, respectively (Weaver et al. 2005). However, the assimilation of Argo trajectory-derived velocities adjusted the

velocity field in a different way, and this assimilation can improve the unbalanced components in velocity increments.

In Exp1, the assimilation of SLA and SST introduce barotropic and baroclinic adjustment on velocity field, among which the barotropic adjustment is dominant and yielded the largest radius of an eddy in Exp1 (Fig. 6b) at approximately 104 km (defined as the distance of model EC to the western boundary). The barotropic and baroclinic geostrophic balance together narrowed the radius of the eddy to 74 km in Exp2 (Fig. 6c). However, the increment of introduced by geostrophic balance is part of the geostrophic current. The radius further decreased to 61 km due to the introduction of the unbalanced components in the velocity increments (Fig. 6d). This increment introduced by assimilating mid-depth velocities is also part of the geostrophic currents through unbalance way not balanced way.

Along with the changes in radius, the position of the EC changed. The EC of Exp3 is obviously closest to the EC of the No. 5903457 float trajectory. The EC in Exp2 is closer than in Exp1, proving that assimilation of *in situ* T/S profile observations is necessary for improving subsurface states. The EC misfits between the model and trajectories are listed in Table 2. The misfit between Exp3 and the observations is the smallest (approximately 0.9 km), followed by Exp2 (approximately 25.6 km). When the balanced components in the velocity increment are overly strong, an opposite correction is made through the introduction of unbalanced components in the velocity increment (Fig. 6e).

The speed of the No. 5903457 float between January 24 and February 2 is smaller than at other times. As shown in Fig. 7, the eddy moved north from January 14th to 26th, and during this time, the float position is closer to the EC but not the edge. Northward movement of EC existed in both Exp2 (Figs. 7a and 7c) and Exp3 (Figs. 7b and 7d). However, the velocity field in Exp3 is more consistent with the observations. Satellite observations contributed to the structure of the velocity field but has little influence on water speed. T/S profiles contribute dominant to the current structure in mid-depth, then mid-depth velocity observation further improved the results.

4.2 Vertical propagation of corrections

The velocity field corrections at ~1200 m are likely to propagate vertically due to the cross-correlation in the background error covariance. Then, these corrections propagate forward through the model dynamic process. This velocity correction propagation in the vertical direction has been studied above the parking depth of the No. 5903457 float (Fig. 8). In Exp2, the eddy structure at different depths is similar, such as the radius and position of EC. The EC distance between 500 m and 1000 m is only 20.9 km, which means that the eddy is almost vertically distributed without tilt. When the mid-depth velocities are assimilated, the radius (especially in the zonal direction) of the eddy decreases with depth, and the EC moves southwest, approaching

the trajectory structure. The EC distance between 500 m and 1000 m increases to 75.5 km in Exp3, which means the EC tilts towards the southwest. The structure of the differences between Exp3 and Exp2 indicated that the speed near the float trajectories is too strong in Exp2, which is corrected in Exp3.The assimilation of the mid-depth velocity also yielded changes in the mass field through a balance operator in the background error covariance. A zonal transect through trajectory EC (111.1°E, 13.8°N) is shown in Fig. 9. In Exp2, a cold core is distributed mainly between 110.5°E and 112°E, which is broader than the diameter of the trajectory (Fig. 6). In Exp3, the cold core diameter is narrowed (between 110.5°E and 111.5°E) and more consistent with the float trajectory. The largest change in the temperature fields (~0.2°C) due to velocity correction is approximately 600 m~1000 m (Fig. 9e), although the float parking depth is approximately 1200 m. The contribution of velocity corrections to the salinity field is on the order of 0.005 PSU (Fig. 9f).

Since our major concern is the western SCS near the eastern coast of the Vietnam, another Argo float (No.5903163) is also in this region. The result of this float has also been check (as shown in Fig. 10 and Fig. 11). It can be seen that the movement of No.5903457 is contrast to the surface velocity, indicating that the eddy in 1200m is not formed in surface. Differ to No.5903457 float, the movement of No.5903163 float is consistent with the trajectory in surface, drifting from northeast to southeast. All assimilation experiments can capture the movement in the surface. However, differences occurred at 1200m (Fig.12). The anti-cyclonic eddy which capture

No.5903457 float moved northward and capture No.5903163 float in Feb, 2013. The northward movement of the anti-cyclonic eddy can been seen in Exp2 and Exp3, but failed in Exp1. The anti-cyclonic eddy in Exp3 moved further toward north than Exp3, so more consistent with the trajectory.

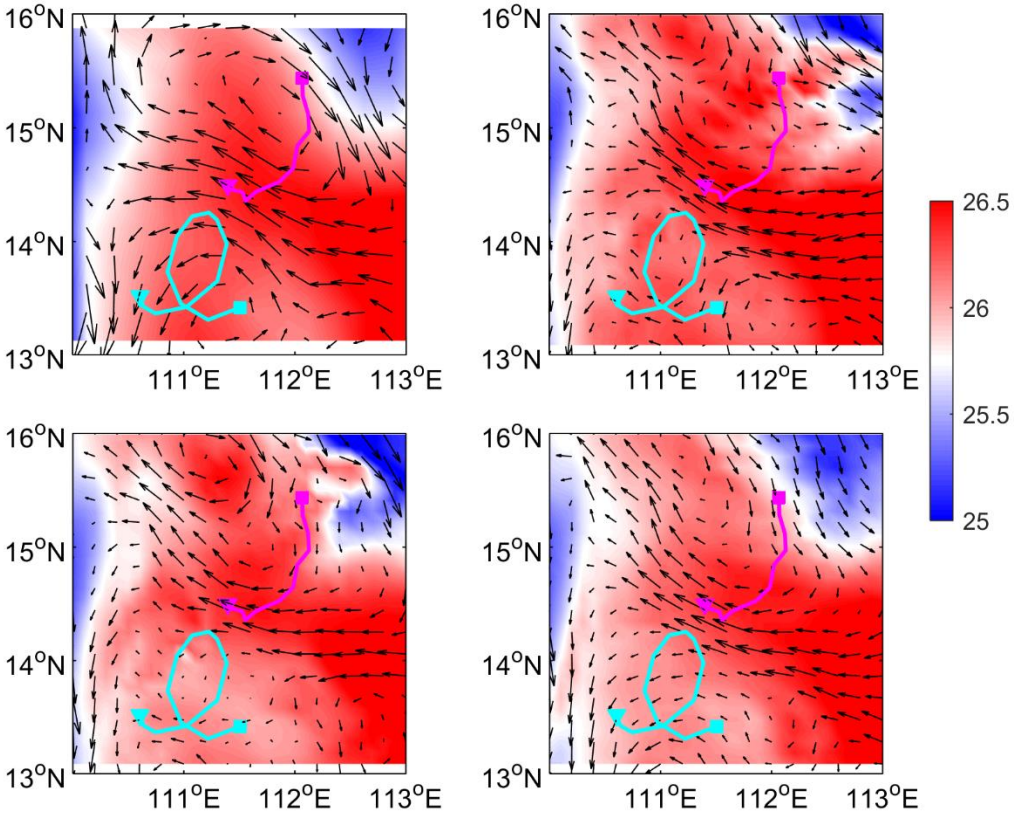

Fig. 10 The SST in 20130115 for a) AVHRR; b) Exp1; c) Exp2; d) Exp3. The vectors are surface geostrophic currents.

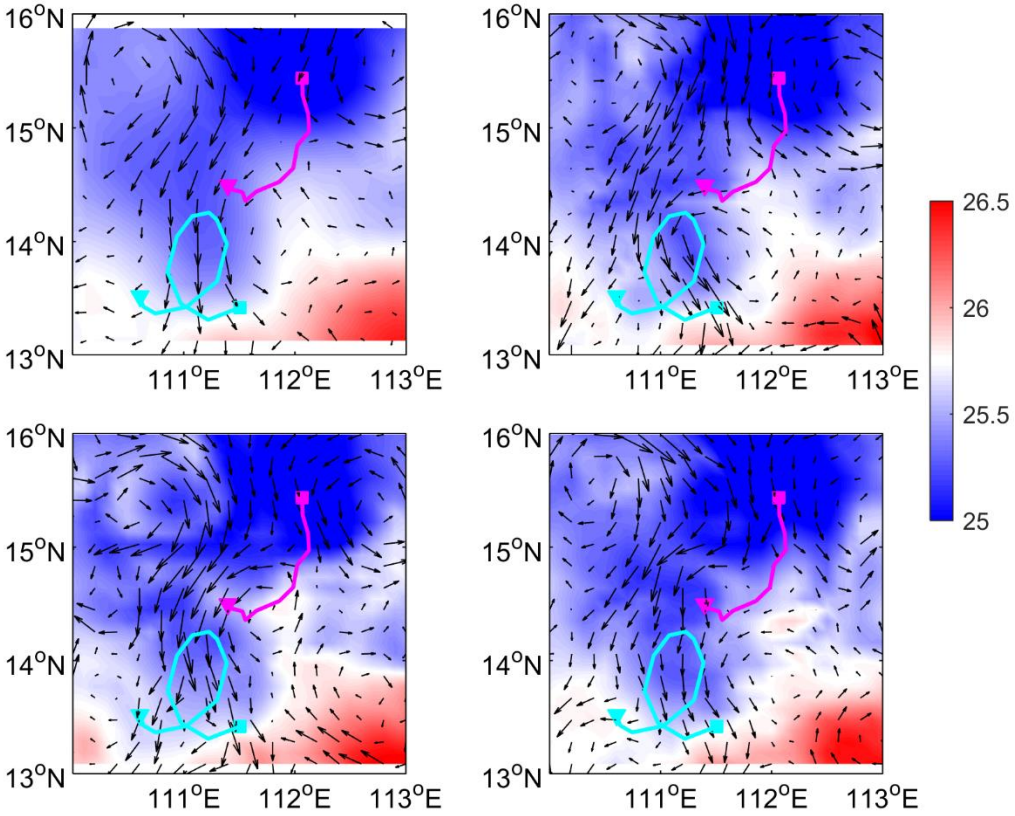

380

381 Fig.11 same as Fig? but for 20130214

382

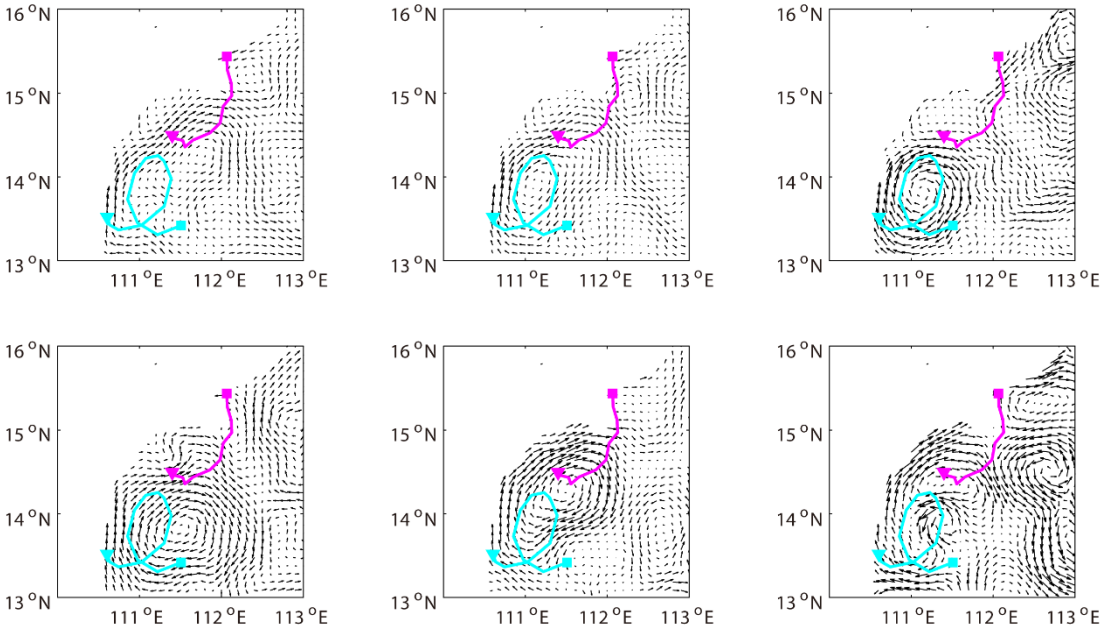

383

384 Fig.12 The velocity field from Exp1(left panel), Exp 2(middle panel) and Exp3

385 (right panel) in 20130115 (upper panel) and 20130214 (bottom panel)

386

387 **4.3 System compatibility**

388 When adding a new dataset, it is important that the forecast quality of the SST,
389 SLA, T profile and S profile not decrease. The compatibility of the trajectory with other
390 observations in the 4DVAR system was checked through statistical analysis. The
391 RMSEs between the model field and observations are defined as follows:

392 $$\mathrm{RMSE}(x) = \sqrt{\sum_{i=1}^{N}\left(x_i^{model} - x_i^{observation}\right)^2 / N} \quad (3)$$

393 where *x* denotes the SST, SLA, T (temperature profile) or S (salinity profile), and
394 *N* is the total number of *x* for 2 months. In terms of SST and SLA, only water depths
395 greater than 200 m are counted.. The 2-month RMSEs in whole region and western
396 SCS in our concern (110-114° E, 13 - 16° N) are shown in Table 3, the assimilation
397 experiments show better performances overall than the Ctrl experiment. The
398 performance of the salinity forecast decreased little when only the satellite observations
399 (SST and SSH) were assimilated. This error is reduced when *in situ* T/S profile data are
400 assimilated. When the additional Argo trajectory-derived mid-depth velocities are
401 introduced, the forecast level of other variables is maintained at the previous levels as
402 in Exp2. The RMSE of the SLA decreased more than in Exp2. This demonstrates that
403 the method we use can effectively assimilate the Argo trajectory into the model without
404 introducing other problems.

405 The biases of T/S are shown in Fig.13 (whole model region) and Fig.14 (western
406 SCS). The assimilation of mid-depth velocities increased the T/S biases in upper 100m

but reduced the T/S biases below 300m. The largest biases and RMSEs occurred about 150m.

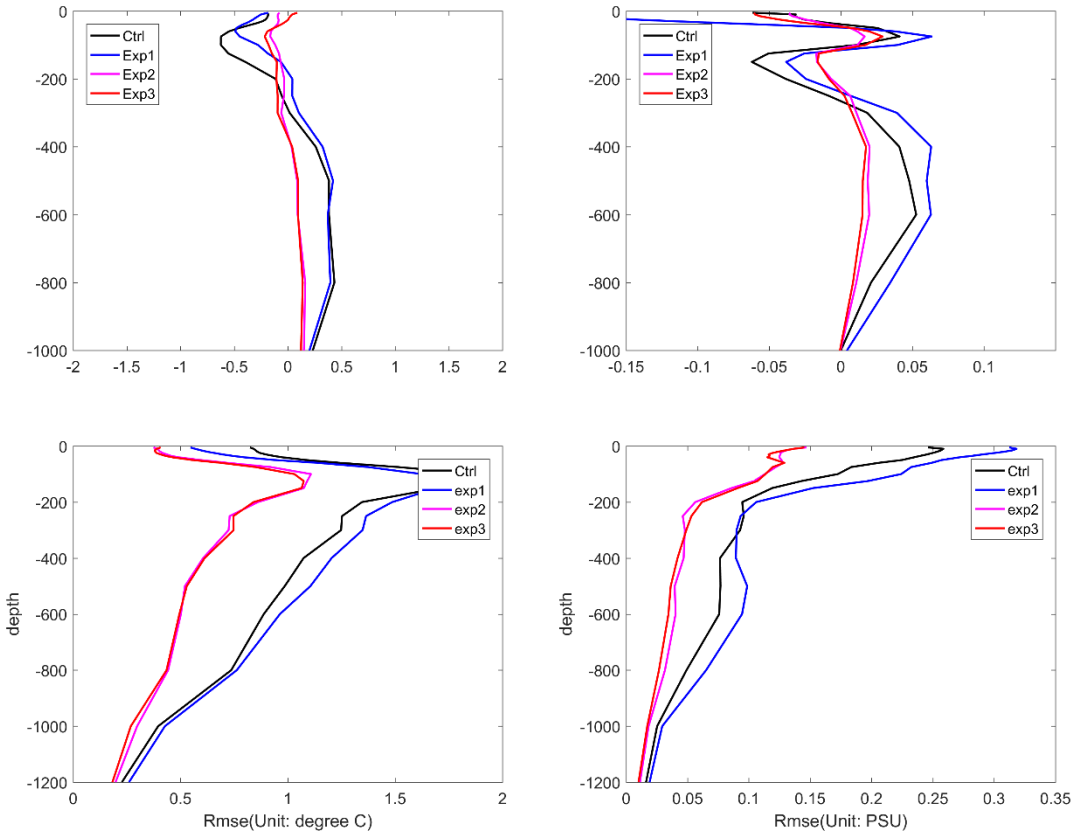

Fig.13 Basin-scale biases (upper panel) and RMSEs (bottom panel) in two months of T(left panel) and S(right panel)

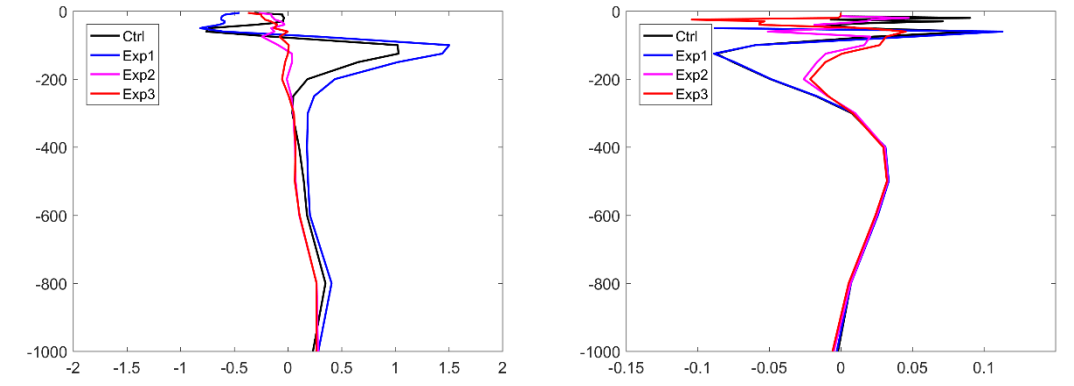

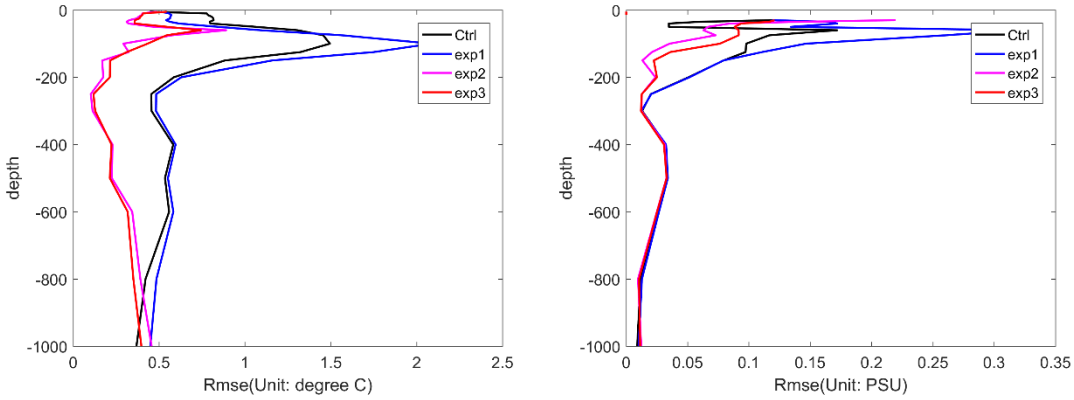

Fig.14 same as Fig.13 but for western SCS near Vietnam (110° E - 113°E, 13°N - 16°N)

Generally, the assimilation of satellite and T/S profile data are not enough to yield accurate modeling of the mid-depth velocity field in the western SCS. Except for balanced information, assimilation of the Argo trajectory can aid in providing additional unbalanced information, which further improves the forecast quality of the velocity fields at the float parking depth.

5 Summary and discussion

Argo trajectory data are useful in studying basin scale current structures in the middle layer of the ocean but are rarely used in ocean data assimilation. In this paper, the Argo trajectory data are assimilated into a regional model of the SCS. Instead of directly assimilating the trajectory data, which requires a complicated trajectory prediction model, the mid-depth velocities are first retrieved from the float trajectories and then assimilated into the ocean model. Before assimilated into the model, the trajectories were subjected to two rounds of quality control, and the observation error of the mid-depth velocities was estimated from the distribution of velocity misfits

between the Argo and HYCOM-NCODA product and finally set to 2 cm/s.

Four experiments were designed to evaluate the influence of the Argo trajectory assimilation on the mid-depth velocity field. A comparison of 2-months of results from four experiments showed that the current structure at a depth of 1200 m east of Vietnam improved when the float trajectory positions were assimilated together with other observations, although the amount of float trajectory positions was small. Accurately modeling the complicated velocity field in the SCS subsurface cannot be adequately accomplished by assimilating only satellite and *in situ* T/S profile observations. The main component of velocity at 1200m is geostrophic current. Mid-depth velocity data assimilation can adjust the unbalanced component of velocity field, which influences the properties of the mesoscale process in the subsurface, such as position and strength. Velocity field corrections are not limited to the observation position at the float parking depth but only propagate horizontally and vertically in a 4DVAR assimilation window. A comparison of Exp2 and Exp3 showed that the velocity field corrections also impact the temperature and salinity fields.The above conclusion is mainly drawn from the No. 5903457 float and No.5902163 in the western SCS near Vietnam but can also be applied to other regions with Argo float trajectories in the SCS (not shown). This finding will be useful for more accurately describing the intermediate velocity in the SCS since and increasing number of Argo floats will be deployed in the SCS, such as the Maritime Silk Road Project. A statistical analysis of the whole region showed that this indirect assimilation method can reduce the T/S biases and RMSEs. It can maintain

the forecast level of other observations and not introduce other problems, such as spurious values in the model states or model blowup.

Some shortcomings remain in this paper. Tides are important progress and can improve the simulation in subsurface () but our model does not include tides. The major problem of including tides in model is the changing for assimilating SLA due to its high frequency variability. Add tides to the model will be considered it further work. The data assimilation system made some simple assumptions as in most ocean data assimilation, including the correlation matrix is isotropic and uniform and observation errors between u and v is uncorrelated. The horizontal and vertical correlation length scales are uniform (50 km horizontally and 30 m vertically), which is one reason why the assimilation of satellite data imposed a larger radius in Exp1 than in the other experiments. The assimilation window is 4D in the assimilation experiments following Moore et al. (2011b), which may not be the optimal assimilation window in the SCS. These drawbacks will be addressed further in future studies.

Acknowledgements

This study was jointly supported by the National Key R&D Program of China （2018YFC1406202）and National Natural Science Foundation of China (41675097, 41830964).

Reference

Atlas, R., R. N. Hoffman, J. Ardizzone, S. M. Leidner, J. C. Jusem, D. K. Smith, and D. Gombos, 2011: A cross-calibrated, multiplatform ocean surface wind velocity product for meteorological and oceanographic applications. *B. Am. Meteorol. S.*, **92**, 157-174, https://doi.org/10.1175/2010BAMS2946.1.

Carton, J. A., G. A. Chepurin, and L. Chen, 2018: SODA3: a new ocean climate reanalysis. *J. Climate*, **31**, 6967-6983, https://doi.org/10.1175/JCLI-D-18-0149.1

Chao, S. Y., P. T. Shaw, and S. Y. Wu, 1996: Deep water ventilation in the South China Sea. *Deep-Sea Res. Pt. I*, **43**, 445-466, https://doi.org/10.1016/0967-0637(96)00025-8.

Chen, G., Y. Hou, and X. Chu, 2011. Mesoscale eddies in the South China Sea: Mean properties, spatiotemporal variability, and impact on thermohaline structure. *J. Geophys. Res. Ocean.*, **116**, https://doi.org/10.1029/2010JC006716.

Chen, G., D. Wang, C. Dong, T. Zu, H. Xue, Y. Shu, X. Chu, Y. Qi, and H. Chen, 2015: Observed deep energetic eddies by seamount wake. *Sci. Rep.*, **5**, 17416, https://doi.org/10.1038/srep17416.

Chu, P. C., and R. Li, 2000: South China Sea isopycnal-surface circulation. *J. Phys. Oceanogr.*, **30**, 2419-2438, https://doi.org/10.1175/1520-0485(2000)030<2419:SCSISC>2.0.CO;2.

Courtier, P., J. N. Thépaut, and A. Hollingsworth, 1994: A strategy for operational

493 implementation of 4D‐Var, using an incremental approach. *Q. J. Roy. Meteor.*
494 *Soc.*, **120**, 1367-1387, https://doi.org/10.1002/qj.49712051912.
495 Dee, D. P., S. M. Uppala, A. J. Simmons, P. Berrisford, P. Poli, S. Kobayashi, U.
496 Andrae, M. A. Balmaseda, G. Balsamo, P. Bauer, P. Bechtold, A. C. M. Beljaars,
497 L. van de Berg, J. Bidlot, N. Bormann, C. Delsol, R. Dragani, M. Fuentes, A. J.
498 Geer, L. Haimberger, S. B. Healy, H. Hersbach, E. V. Hólm, L. Isaksen, P.
499 Kållberg, M. Köhler, M. Matricardi, A. P. McNally, B. M. Monge‐Sanz, J.‐J.
500 Morcrette, B.‐K. Park, C. Peubey, P. de Rosnay, C. Tavolato, J.‐N. Thépaut,
501 and F. Vitart, 2011: The ERA‐Interim reanalysis: Configuration and
502 performance of the data assimilation system. *Q, J, Roy. Meteor. Soc.*, **137**, 553-
503 597, https://doi.org/10.1002/qj.828.
504 Fang, G., G. Wang, Y. Fang, and W. Fang, 2012: A review on the South China Sea
505 western boundary current. *Acta Oceanol. Sin.*, **31**, 1-10,
506 https://doi.org/10.1007/s13131-012-0231-y.
507 Good, S. A., M. J. Martin, and N. A. Rayner, 2013: EN4: Quality controlled ocean
508 temperature and salinity profiles and monthly objective analyses with uncertainty
509 estimates. *J. Geophys. Res. Ocean.*, **118**, 6704-6716,
510 https://doi.org/10.1002/2013JC009067.
511 Hu, J., H. Kawamura, H. Hong, and Y. Qi, 2000: A review on the currents in the South
512 China Sea: seasonal circulation, South China Sea warm current and Kuroshio
513 intrusion. *J. Oceanogr.*, **56**, 607-624, https://doi.org/10.1023/A:1011117531252.

514 Lebedev, K. V., H. Yoshinari, N. A. Maximenko, and P. W. Hacker, 2007: Velocity
515 data assessed from trajectories of Argo floats at parking level and at the sea surface.
516 IPRC *Tech. Note*, **4**, https://doi.org/10.13140/RG.2.2.12820.71041.
517 Li, J., R. Zhang, and B. Jin, 2011: Eddy characteristics in the northern South China Sea
518 as inferred from Lagrangian drifter data. *Ocean Sci.*, **7**, 661,
519 https://doi.org/10.5194/os-7-661-2011.
520 Liao, G., Y. Yuan, and X. Xu, 2005: The three dimensional structure of the circulation
521 in the South China Sea during the winter of 1998. *Acta Oceanol. Sin.*, **27**, 8-17.
522 (In Chinese).
523 Lin, X., C. Dong, D. Chen, Y. Liu, J. Yang, B. Zou, and Y. Guan, 2015: Three-
524 dimensional properties of mesoscale eddies in the South China Sea based on eddy-
525 resolving model output. *Deep-Sea Res. Pt. I*, 2015, **99**, 46-64,
526 https://doi.org/10.1016/j.dsr.2015.01.007.
527 Liu, Q., A. Kaneko, and J. Su, 2008: Recent progress in studies of the South China Sea
528 circulation. *J. Oceanogr.*, **64**: 753-762, https://doi.org/10.1007/s10872-008-0063-
529 8.
530 Markova, N. V., and A. V. Bagaev, 2016. The Black Sea Deep Current Velocities
531 Estimated from the Data of Argo Profiling Floats. *Phys. Oceanogr.*, **3**,
532 https://doi.org/10.22449/1573-160X-2016-3-23-35.
533 Moore, A. M., H. G. Arango, G. Broquet, B. S. Powell, A. T. Weaver, and J. Zavala-
534 Garay, 2011a: The Regional Ocean Modeling System (ROMS) 4-dimensional

variational data assimilation systems: Part I–System overview and formulation. *Prog. Oceanogr.*, **91**: 34-49, https://doi.org/ 10.1016/j.pocean.2011.05.004.

Moore, A. M., H. G Arango, G. Broquet, C. Edwards, M. Veneziani, B. Powell, D. Foley, J. D. Doyle, D. Costa and P. Robinson, 2011b: The Regional Ocean Modeling System (ROMS) 4-dimensional variational data assimilation systems: part II–performance and application to the California Current System. *Prog. Oceanogr.*, **91**, 50-73, https://doi.org/10.1016/j.pocean.2011.05.003.

Nilsson, J. A. U., S. Dobricic, N. Pinardi, P.-M. Poulain, and D. Pettenuzzo, 2012: Variational assimilation of Lagrangian trajectories in the Mediterranean ocean Forecasting System. *Ocean Sci*, **8**, 249-259, https://doi.org/10.5194/os-8-249-2012.

Nilsson, J. A. U., S. Dobricic, N. Pinardi, V. Taillandier, and P.-M. Poulain, 2011: On the assessment of Argo float trajectory assimilation in the Mediterranean Forecasting System. *Ocean Dynam.*, **61**, 1475-1490, https://doi.org/10.1007/s10236-011-0437-0.

Ollitrault, M., and J. P. Rannou, 2013: ANDRO: An Argo-based deep displacement dataset. *J. Atmos. Oceanic Technol.*, **30**, 759-788, https://doi.org/10.1175/JTECH-D-12-00073.1

Ollitrault, M., and Colin de Verdière A., 2014: The ocean general circulation near 1000-m depth. *J. Phys. Oceanogr.*, **44**: 384-409, https://doi.org/10.1175/JPO-D-13-030.1.

556 Park, J. J., K. Kim, and W. R. Crawford, 2004: Inertial currents estimated from surface
557 trajectories of ARGO floats. *Geophys. Res. Lett.*, **31**,
558 https://doi.org/10.1029/2004GL020191.
559 Park, J. J., K. Kim, B. A. King, and S. C. Riser, 2005: An advanced method to estimate
560 deep currents from profiling floats. *J. Atmos. Oceanic Technol.*, **22**: 1294-1304,
561 https://doi.org/10.1175/JTECH1748.1.
562 Park, J. J. and K. Kim, 2013: Deep currents obtained from Argo float trajectories in the
563 Japan/East Sea. *Deep-Sea Res. Pt II*, 2013, **85**: 169-181,
564 https://doi.org/10.1016/j.dsr2.2012.07.032.
565 Quan, Q., H. Xue, H. Qin, X. Zeng, S. Peng, 2016: Features and variability of the South
566 China Sea western boundary current from 1992 to 2011. *Ocean Dynam.*, **66**, 795-
567 810, https://doi.org/10.1007/s10236-016-0951-1.
568 Song, B., H. Wang, C. Chen, S. Bao, and R. Zhang, 2018: Observed subsurface eddies
569 near the Vietnam coast of the South China Sea. *Acta Oceanol. Sin.* (in press).
570 Reynolds, R. W., T. M. Smith, C. Liu, C., D. B. Chelton, K. S. Casey, and M. G. Schlax,
571 2007: Daily high-resolution-blended analyses for sea surface temperature. *J.*
572 *Climate*, **20**: 5473-5496, https://doi.org/10.1175/2007JCLI1824.1.
573 Taillandier, V., A. Griffa, P. M. Poulain, and K. Béranger, 2006a: Assimilation of Argo
574 float positions in the north western Mediterranean Sea and impact on ocean
575 circulation simulations. *Geophys. Res. Lett.*, **33**,
576 https://doi.org/10.1029/2005GL025552.

577 Taillandier, V., and A. Griffa, 2006b: Implementation of position assimilation for
578 ARGO floats in a realistic Mediterranean Sea OPA model and twin experiment
579 testing. *Ocean Sci.*, **3**, 255-289, https://doi.org/10.5194/os-2-223-2006.
580 Voet, G., D. Quadfasel, K. A. Mork, and H. Søiland, 2010: The mid-depth circulation
581 of the Nordic Seas derived from profiling float observations. *Tellus A*, **62**, 516-
582 529, https://doi.org/10.1111/j.1600-0870.2009.00444.x.
583 Wang, D., Q. Liu, Q. Xie, Z. He, W. Zhuang, Y. Shu, X. Xiao, B. Hong, X. Wu, and D.
584 Sui, 2013: Progress of regional oceanography study associated with western
585 boundary current in the South China Sea. *Chin. Sci. Bull.*, **58**: 1205-1215,
586 https://doi.org/10.1007/s11434-012-5663-4.
587 Wang, G., J. Su, and P. C. Chu, 2003: Mesoscale eddies in the South China Sea
588 observed with altimeter data. *Geophys. Res. Lett.*, 2003, **30**,
589 https://doi.org/10.1029/2003GL018532.
590 Wang, H., G. Wang, D. Chen, and R. Zhang, 2012a: Reconstruction of Three-
591 Dimensional Pacific Temperature with Argo and Satellite Observations. *Atmos.*
592 *Ocean*, **50**,116-128, https://doi.org/10.1080/07055900.2012.742421.
593 Wang, H., R. Zhang, Wang G, Y. An, and B. Jin, 2012b: Quality control of Argo
594 temperature and salinity observation profiles. *Chinese J. Geophys.*, **55**, 577-588,
595 https://doi.org/10.6038/j.issn.0001-5733.2012.02.020.(in Chinese)
596 Wang, X., W. Zhang, P. Wang, J. Yang, and H. Wang, 2018: Research on mid-depth
597 current of basin scale in the South China Sea based on historical Argo observations.

598 Haiyang Xuebao, **40**, 1-14, https://doi.org/10.3969/j.issn.0253-4193.2018.06.001.
599 (in Chinese)
600 Warner, J. C., C. R. Sherwood, H. G. Arango, and R. P. Signell, 2005: Performance of
601 four turbulence closure models implemented using a generic length scale method.
602 *Ocean Model.*, **8**, 81-113, https://doi.org/10.1016/j.ocemod.2003.12.003.
603 Weaver, A. T., C. Deltel, Machu É, S. Ricci, and N. Daget, 2005. A multivariate balance
604 operator for variational ocean data assimilation. *Q.J.R. Meteorol. Soc.*, **131**, 3605-
605 3625, https://doi.org/10.1256/qj.05.119.
606 Weaver, A. T., J. Vialard, and D. L. T. Anderson, 2003: Three-and four-dimensional
607 variational assimilation with a general circulation model of the tropical Pacific
608 Ocean. Part I: Formulation, internal diagnostics, and consistency checks. *Mon.*
609 *Wea. Rev.*, **131**, 1360-1378, https://doi.org/10.1175/1520-
610 0493(2003)131<1360:TAFVAW>2.0.CO;2.
611 Wyrtki, K., 1961: Physical oceanography of the Southeast Asian waters. *UC San Diego:*
612 *Scripps Institution of Oceanography*. Retrieved from
613 https://escholarship.org/uc/item/49n9x3t4.
614 Xie, J., and J. Zhu, 2008: Estimation of the surface and mid-depth currents from Argo
615 floats in the Pacific and error analysis. *J. Marine Sys.*, **73**, 61-75,
616 https://doi.org/10.1016/j.jmarsys.2007.09.001.
617 Xiu, P., F. Chai, L. Shi, H. Xue, and Y. Chao, 2010: A census of eddy activities in the
618 South China Sea during 1993–2007. *J. Geophys. Res.*, 2010, **115**,

https://doi.org/10.1029/2009JC005657.

Yuan, D., 2012: A numerical study of the South China Sea deep circulation and its relation to the Luzon Strait transport. *Acta Oceanol. Sin.*, **21**, 187-202.

Zhang, Z., F. Qiao, and J. Guo, 2014: Subsurface eddies in the southern South China Sea detected from in-situ observation in October 2011. *Deep-Sea Res. Pt. I*, **87**, 30-34, https://doi.org/10.1016/j.dsr.2014.02.004.

Zhang, Z., J. Tian, B. Qiu, W. Zhao, P. Chang, D. Wu, and X. Wan, 2016: Observed 3D structure, generation, and dissipation of oceanic mesoscale eddies in the South China Sea. *Sci. Rep.*, **6**, 24349, https://doi.org/10.1038/srep24349.

Zhou, H., D. Yuan, R. Li, and L. He, 2010: The western South China Sea currents from measurements by Argo profiling floats during October to December 2007. *Chin. J. Ocean. Limnol.*, **28**, 398-406, https://doi.org/10.1007/s00343-010-9052-z.

Tables

Table 1. Table 1 Experimental design

Exp. Name	SST	SLA	T/S	VEC
Ctrl	N	N	N	N
Exp1	Y	Y	N	N
Exp2	Y	Y	Y	N
Exp3	Y	Y	Y	Y

Note: The assimilated observations are marked with Y; otherwise, the observations are marked with N. SST (satellite SST), SLA (sea level anomaly observation), T (*in situ* temperature profile), S (*in situ* salinity profile), and VEC (velocity derived from Argo trajectory).

Table 2. RMS misfits between model values and observations at 1200 m for EC, u and v. The CCs are displaced within the brackets

	Ctrl	Exp1	Exp2	Exp3
EC (km)	87.7	54.1	25.6	0.9
U (cm/s)	6.1 (-0.15)	6.1 (0.22)	3.9 (0.81)	3.2 (0.87)
V (cm/s)	7.2 (0.06)	10.9 (-0.51)	7.7 (0.58)	2.5 (0.94)

Note: The eddy center from the model output (EC) is the location of the minimum speed in the eddy. The EC (111.1°E, 13.8°N) of the trajectory observations is identified by 8 nearly symmetrical points (3, 4, 5, 6, 8, 9, 10 and 11 in Fig. 3b) of the trajectory, i.e., the position where the sum of the distance to these points is the shortest.

649 **Table 3.** Two-month basin-averaged RMSEs between model fields.

	Ctrl		Exp1		Exp2		Exp3	
	Whole	WBC	Whole	WSCS	Whole	WSCS	Whole	WSCS
SST (°C)	0.88	1.0	0.26	0.15	0.27	0.19	0.27	0.2
SLA (cm)	8.6	6.6	4.1	2.3	5.1	2.9	4.8	2.7
T(°C)	0.86	0.86	0.81	0.92	0.65	0.38	0.65	0.37
S(PSU)	0.23	0.06	0.32	0.11	0.17	0.03	0.17	0.04

650

Figure Caption List

Fig. 1. Distribution of velocity deviation between HYCOM-NCODAproduct and Argo data at 1200 m during 2006~2016. (Blue is the distribution of zonal ocean current *u*, and green is the distribution of meridional ocean current *v*).

Fig. 2. RMSEs and CCs of *u* and *v* for different observation error standard deviations in Jan and Feb, 2013. The red line represents 2 cm/s, and the blue line represents 5 cm/s.

Fig. 3. Bathymetry (unit: m) and model domain (99°E~134°E, 1°N~30°N). The black contour represents the 200 m isobath. TW represents Taiwan Island.

Fig. 4. Distribution of mid-depth velocities (a) and No. 5903457 Argo float T/S profile position (b) during 1 Jan-28 Feb, 2013. The range in (b) is marked by a black box in (a); the number in (b) represents the observational sequence in the first 2 months of 2013.

Fig. 5. Two-month averaged velocity field from (a) Ctrl, (b) Exp1, (c) Exp2, (d) Exp3 and (e) the difference between Exp3 and Exp2. The No. 5903457 float trajectory is represented by the magenta line, the starting position of the float in January is represented by the magenta square, the final position is represented by the triangle, and the center is represented by the magenta pentagram. The EC in the model fields is represented by a black pentagram.

Fig. 6. Comparison of the velocity field between Exp2 (left panel) and Exp3 (right panel) on Jan 14, 2013 (top panel) and Jan 26, 2013 (bottom panel). The red vector represents

the mid-depth velocity from the float trajectory (unit: cm/s).

Fig. 7. Two-month average velocity field of Exp2 (left), Exp3 (middle) and the difference between them (right, Exp3-Exp2). Top is 500 m, middle is 750 m and bottom is 1000 m. Contours represent stream function (interval 2000, unit: m^3/s). No. 5903457 float trajectory is represented by the magenta line.

Fig. 8. Temperature (left) and salinity (right) zonal transects (along 13.8°N) of the difference between Exp2 and Ctrl (top panel), the difference between Exp3 and Ctrl (middle panel) and the difference between Exp3 and Exp2 (bottom panel).

Figure

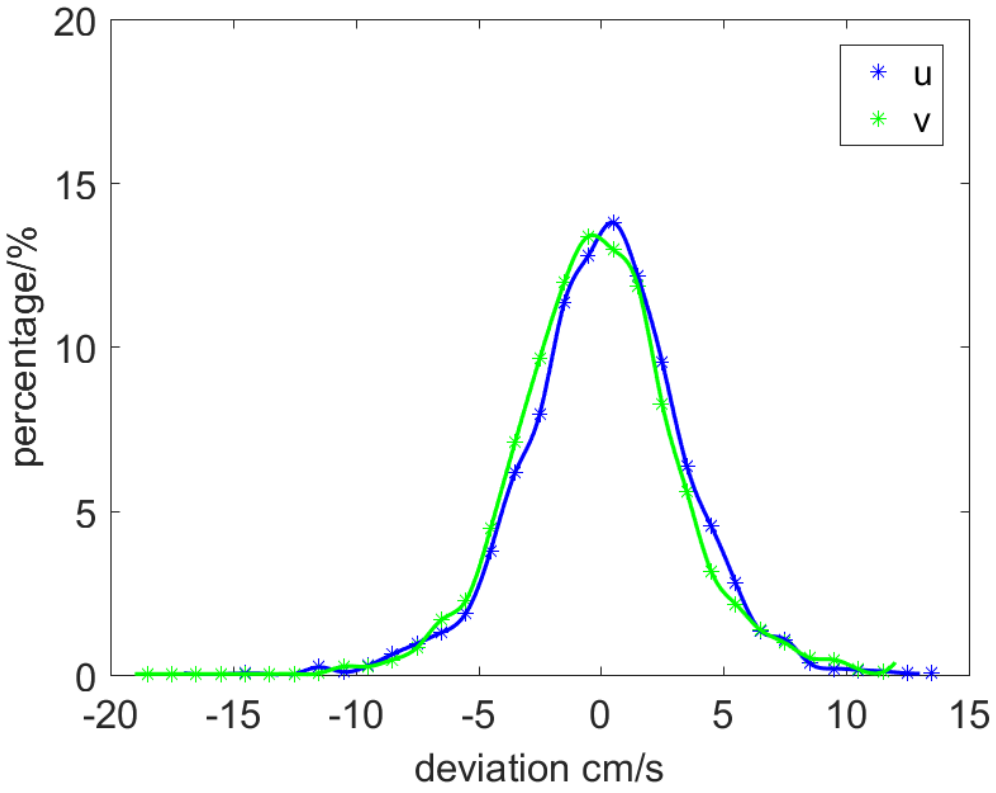

Fig. 1. Distribution of velocity deviation between HYCOM-NCODA product and Argo data at 1200 m during 2006~2016. (Blue is the distribution of zonal ocean current *u*, and green is the distribution of meridional ocean current *v*).

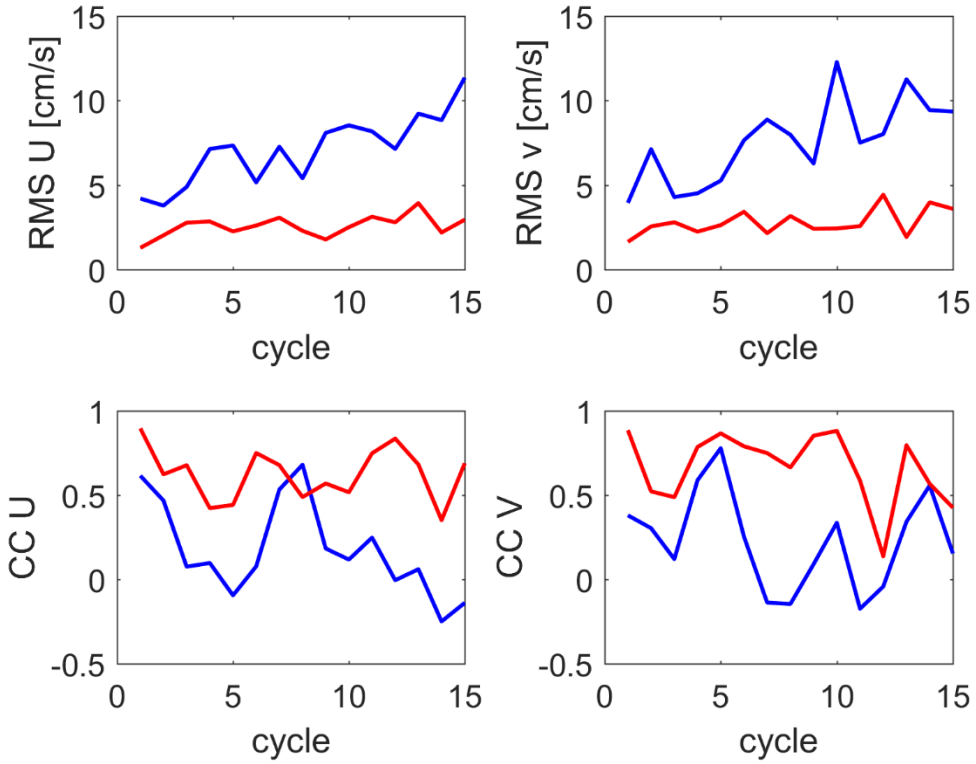

686

687 **Fig. 2.** RMSEs and CCs of *u* and *v* for different observation error standard deviations
688 in Jan and Feb, 2013. The red line represents 2 cm/s, and the blue line represents 5 cm/s.
689

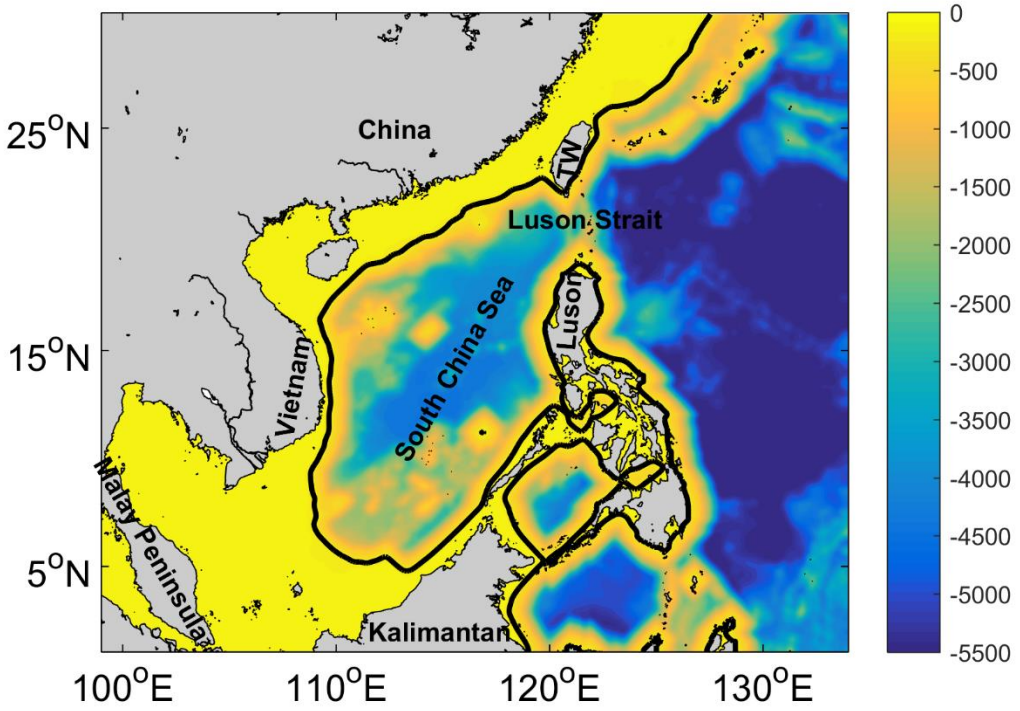

690

691 **Fig. 3.** Bathymetry (unit: m) and model domain (99°E~134°E, 1°N~30°N). The black
692 contour represents the 200 m isobath. TW represents Taiwan Island.
693

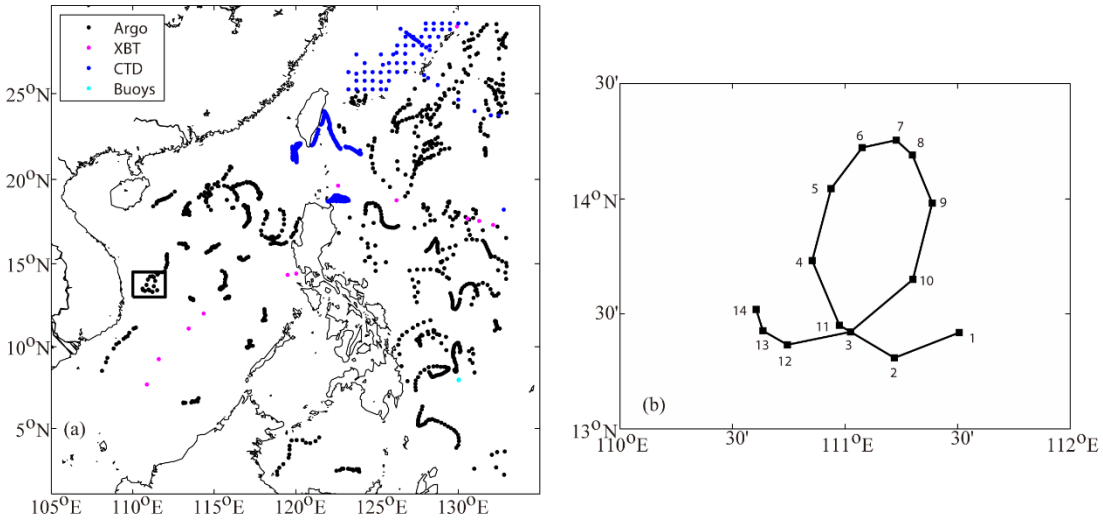

694
695 **Fig. 4.** Distribution of in-situ observations (a) and No. 5903457 Argo float T/S profile
696 position (b) during 1 Jan-28 Feb, 2013. The range in (b) is marked by a black box in
697 (a); the number in (b) represents the observational sequence in the first 2 months of
698 2013.
699

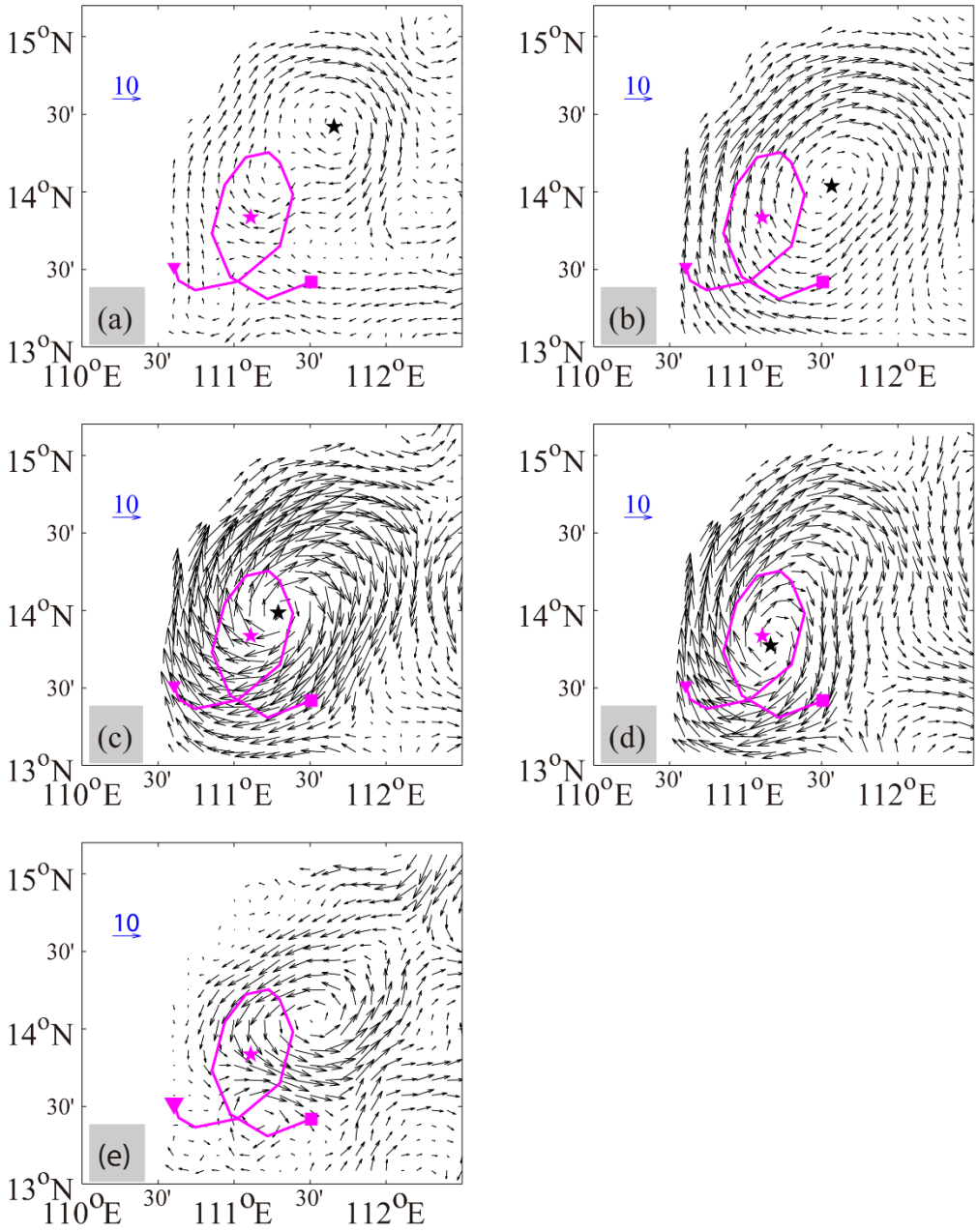

Fig. 5. Two-month averaged velocity field from (a) Ctrl, (b) Exp1, (c) Exp2, (d) Exp3 and (e) the difference between Exp3 and Exp2. The No. 5903457 float trajectory is represented by the magenta line, the starting position of the float in January is represented by the magenta square, the final position is represented by the triangle, and the center is represented by the magenta pentagram. The EC in the model fields is represented by a black pentagram.

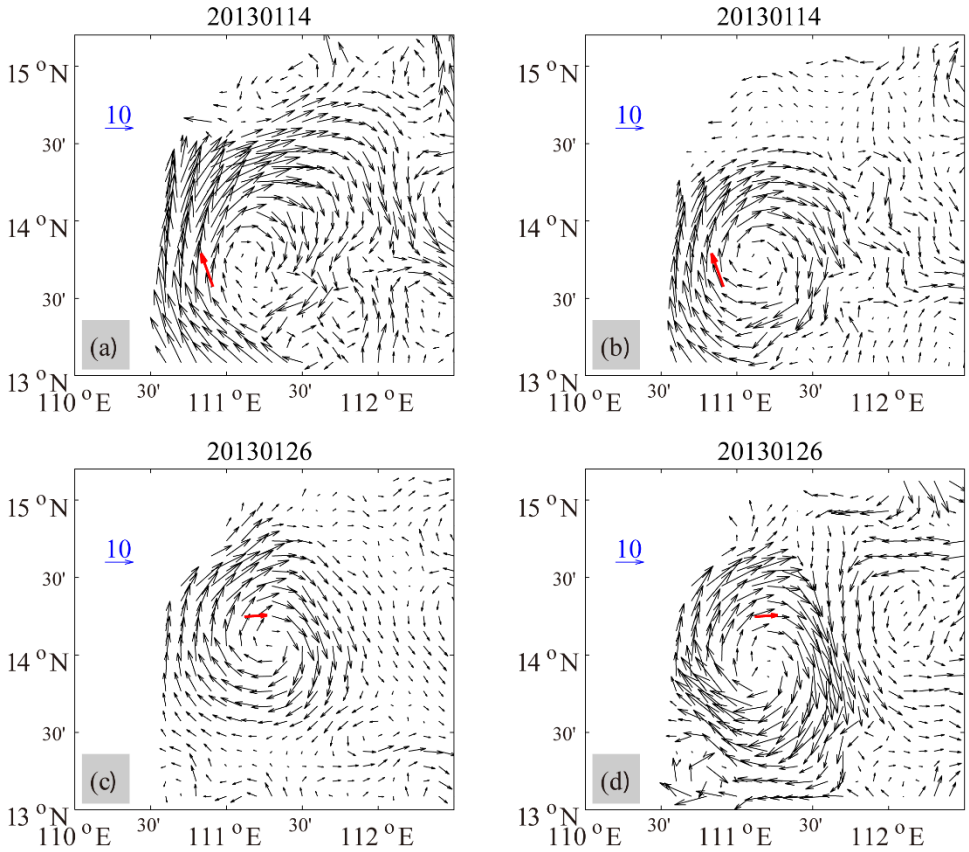

Fig. 6. Comparison of the velocity field between Exp2 (left panel) and Exp3 (right panel) on Jan 14, 2013 (top panel) and Jan 26, 2013 (bottom panel). The red vector represents the mid-depth velocity from the float trajectory (unit: cm/s).

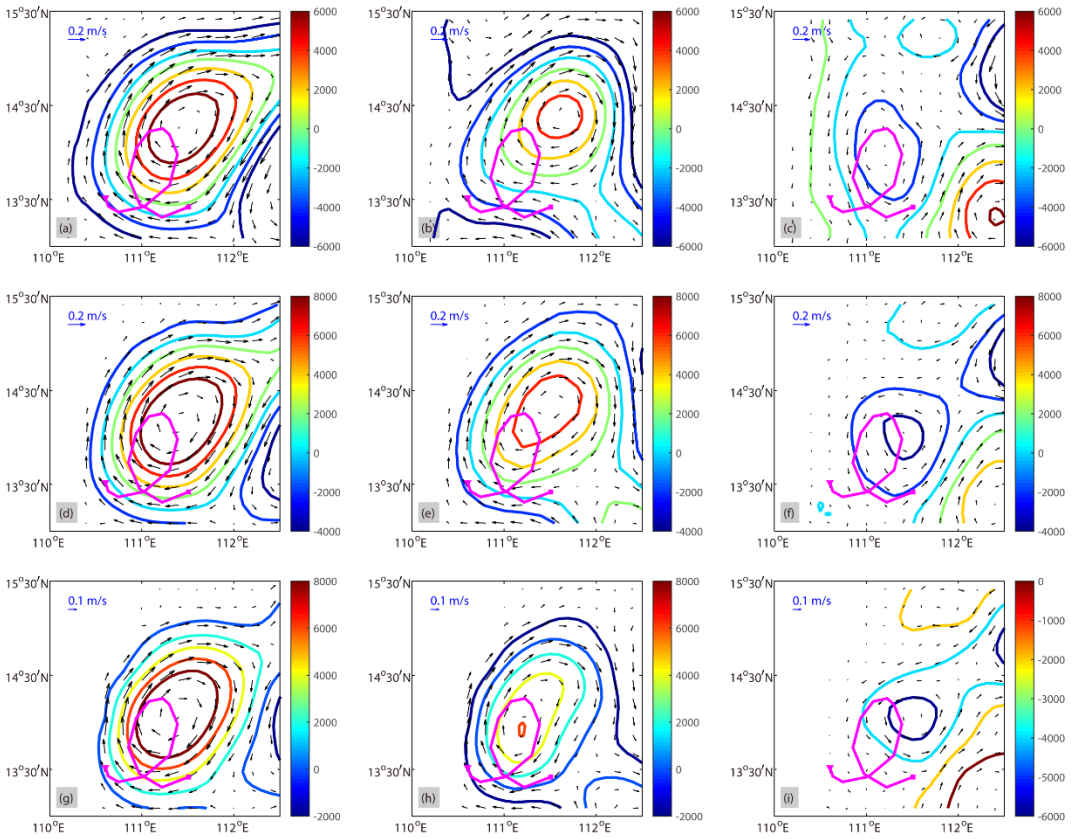

713

714 **Fig. 7.** Two-month average velocity field of Exp2 (left), Exp3 (middle) and the
715 difference between them (right, Exp3-Exp2). Top is 500 m, middle is 750 m and bottom
716 is 1000 m. Contours represent stream function (interval 2000, unit: m^3/s). No. 5903457
717 float trajectory is represented by the magenta line.
718

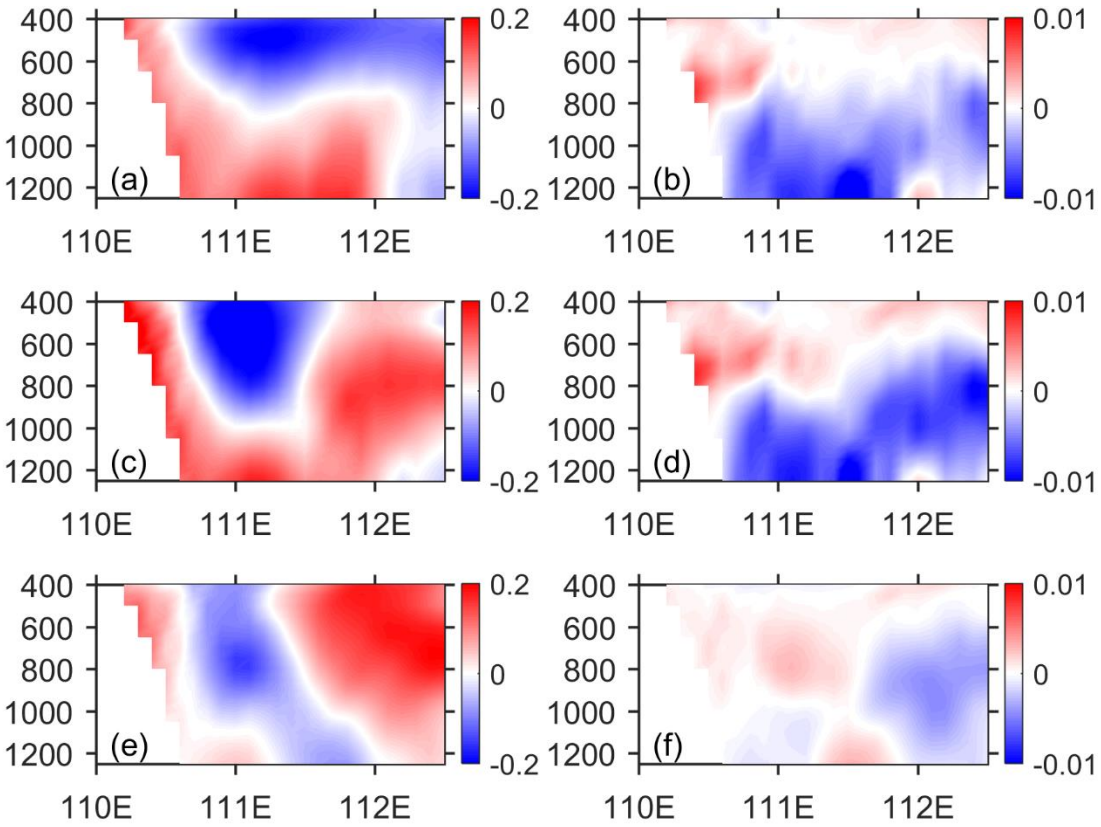

719

720 **Fig. 8.** Temperature (left) and salinity (right) zonal transects (along 13.8°N) of the
721 difference between Exp2 and Ctrl (top panel), the difference between Exp3 and Ctrl
722 (middle panel) and the difference between Exp3 and Exp2 (bottom panel).

723